OPEN ACCESS

Int. J. Creative Res. Publ. *Peer-Reviewed Journal* *Volume 1 Issue 4[Jul-Aug] 2026*

IJCRP

International Journal of Creative Research and Publications

Double Blind Peer Reviewed Journal

Research Article

$Na_2Ti_3O_7$ Ceramics: A Review on Doping-Induced Structural, Dielectric, And Charge Transport Dynamics

Rakesh Singh

Department of Physics, Jagran College of Arts, Science & Commerce, Kanpur, Uttar Pradesh, India

Corresponding Author: *Rakesh Singh

DOI: https://doi.org/10.5281/zenodo.21902979

Abstract

In this study, layered sodium tri-titanate ($Na_2Ti_3O_7$) ceramics doped with 1.0 mol % transition metals (copper, iron, and manganese) were synthesised using a solid-state reaction method. X-ray diffraction confirmed that all samples retained a single-phase monoclinic crystal structure. Replacing the smaller host Ti^{4+} ions with larger dopant cations (Cu^{2+}, $Mn^{2+/3+}$, Fe^{3+}) expanded the interlayer spacing, shifting the primary reflection peaks to lower 2θ angles. Temperature-dependent dielectric testing at 1 MHz revealed that doping creates charge-compensating oxygen vacancies, which lower the activation energy for dipole rotation and cause relaxation peak temperatures to drop systematically (Cu: 600 K < Fe: 612 K < Mn: 622 K < Pure: 635 K). Copper (Cu^{2+}) doping generated the highest relative permittivity (ε' ≈ 770), though with increased energy losses. Electrical conductivity studies demonstrated four distinct temperature regions, showing a transition from low-temperature electronic hopping between Ti^{3+}/Ti^{4+} states to high-temperature fast Na^{+} ion flow quickly through the layer pathways. Overall, these small chemical changes provide an effective way to improve material performance. They offer capable opportunities for developing advanced materials for sodium-ion batteries and high-temperature energy storage applications.

Manuscript Information

- **ISSN No:** 3139-6313
- **Received:** 13-07-2026
- **Accepted:** 03-08-2026
- **Published:** 12-08-2026
- **IJCRP:** 1(4); 2026: 107-112
- **©2026, All Rights Reserved**
- **Plagiarism Checked:** Yes
- **Peer Review Process:** Yes

How to Cite this Article

Singh R. $Na_2Ti_3O_7$ Ceramics: A Review on Doping-Induced Structural, Dielectric, And Charge Transport Dynamics. Int. J. Creative Res. Publ. 2026;1(4):107-112.

Access this Article Online

www.jcrp.in

KEYWORDS: $Na_2Ti_3O_7$ ceramics; Transition metal (Mn, Fe, Cu) doped titanates; XRD pattern comparison; Loss tangent (tan δ); Relative permittivity (ε'); A.C. conductivity; 4-Region Arrhenius model.

1. INTRODUCTION

Polycrystalline layered alkali titanates follow the general chemical formula $A_2Ti_nO_{2n+1}$, where 'A' represents an alkali metal cation (Na^+, K^+, or Li^+) [1, 2] and 'n' typically ranges from 3 to 6 [1, 2]. Over the past six decades, these materials have drawn significant attention as a crucial class of functional electroceramics owing to their anisotropic layer-type framework, high thermal stability, and robust chemical endurance [3, 4]. Strategic tuning of their electrical, dielectric, and ion-exchange dynamics makes layered titanates highly attractive candidates for high-temperature energy storage devices, solid-state sodium battery electrolytes, microwave resonators, and photocatalytic systems [5, 6].

The foundational crystal structure of sodium trititanate ($Na_2Ti_3O_7$) was established by S. Anderson and A. D. Wadsley using single-crystal X-ray diffraction techniques [1, 2]. Pristine $Na_2Ti_3O_7$ crystallizes in a monoclinic unit cell (space group $P2_1/m$) with lattice parameters a = 9.128 Å, b = 3.803 Å, c = 8.566 Å, and β = 101.58° [1, 2]. The structural framework consists of corrugated blocks of edge-sharing TiO_6 octahedra, where three octahedra join along their edges to form stepped units [1]. These blocks share corners to construct open two-dimensional channels occupied by sodium ions residing in two distinct crystallographic sites: 9-fold coordinated Na(1) and 7-fold coordinated Na(2) [2, 5].

Due to the intrinsic monoclinic symmetry, central Ti^{4+} ions experience off-center displacements within the distorted TiO_6 octahedra [5]. This off-centering generates permanent electric dipole moments ranging from 5.0 D to 6.2 D [5, 6]. While these dipoles remain rigidly locked within the oxide matrix at room temperature, thermal activation or externally applied electric fields enable dipolar reorientation and alignment [6, 7]. This reorientation mechanism gives rise to broad, temperature-dependent dielectric relaxation peaks and enhanced polarizability in the ceramic matrix [7, 8].

To model the underlying charge transport and dielectric phenomena, several fundamental transport theories have been established [3, 4]. A. K. Jonscher formulated the Universal Dielectric Response (UDR) model [$\sigma_{ac}(\omega) = \sigma_{dc}+A\omega^s$], describing frequency-dependent a.c. conductivity in disordered solids [3]. Concurrently, S. R. Elliott proposed the Correlated Barrier Hopping (CBH) model, predicting a temperature-dependent decrease in the exponent s as charge carriers hop across defect energy barriers [4]. Later, S. Kikkawa and co-workers demonstrated that interlayer channel dimensions govern the activation barriers for mobile Na^+ ions, facilitating rapid 2D ionic transport at high temperatures [5].

Isovalent or aliovalent substitution at host Ti^{4+} octahedral sites with 3d transition metal cations (Fe^{3+}, $Mn^{2+}/^{3+}$, and Cu^{2+}) significantly modulates the lattice parameters and charge transport dynamics [6, 7]. Incorporating lower-valence dopants generates charge-compensating oxygen vacancies, lowering the energy barriers for dipole rotation and boosting a.c. conductivity [6, 7]. In particular, substituting Ti^{4+} (0.605 Å) with larger active Cu^{2+} ions (0.730 Å) induce prominent octahedral distortions, yielding enhanced dielectric permittivity and modified activation energies [7, 8].

Recent studies have further refined the understanding of structural, defect, and transport dynamics in modified titanates [9, 10]. Structural investigations reveal that octahedral oriented directly sets the physical dimensions of alkali transport channels [9], while Density Functional Theory (DFT) confirm the localized defect states within the 3.49 eV band gap that facilitate low-temperature polaron hopping [10]. Further research links larger dopant radii to unit cell expansion [11], defect dipole-driven relaxation peaks [12], oxygen vacancy-assisted ionic conduction [13], and long-range Na^+ polaron hopping mechanisms [14]. Furthermore, advances in high-temperature capacitor applications [15], high-frequency bulk relaxation isolation [16], and defect engineering [17] draw attention to the growing technological importance of layered titanates.

Despite extensive individual reports, a unified comparative review synthesizing pure and 1 mol% (Mn, Fe, Cu) doped $Na_2Ti_3O_7$ ceramics remains essential. This review provides a wide-ranging analysis covering: (1) XRD full-range patterns and peak-shift dynamics against the Anderson & Wadsley baseline [1, 2], (2) temperature-dependent loss tangent (tan δ) spectra at 1 MHz [6–8], (3) relative permittivity (ε') relaxation profiles [6–8], and (4) a 4-region Arrhenius a.c. conductivity model detailing charge transport from low-temperature electronic hopping to high-temperature fast interlayer Na^+ ionic conduction [4, 6–8].

2. X-Ray Diffraction (XRD) Structural Comparison: Pure versus 1 mol% Doped Ceramics

Figure 1A display the full-range XRD patterns (2-theta = 8 deg to 60 deg) comparing Pure $Na_2Ti_3O_7$ [1, 2] against 1 mol% Mn, Fe, and Cu doped derivatives [6–8]. Figure 1B provides a magnified view of the primary (200) interlayer reflection at 2-theta ~ 10.60 deg to highlight the exact Bragg peak shift [1, 2, 6–8].

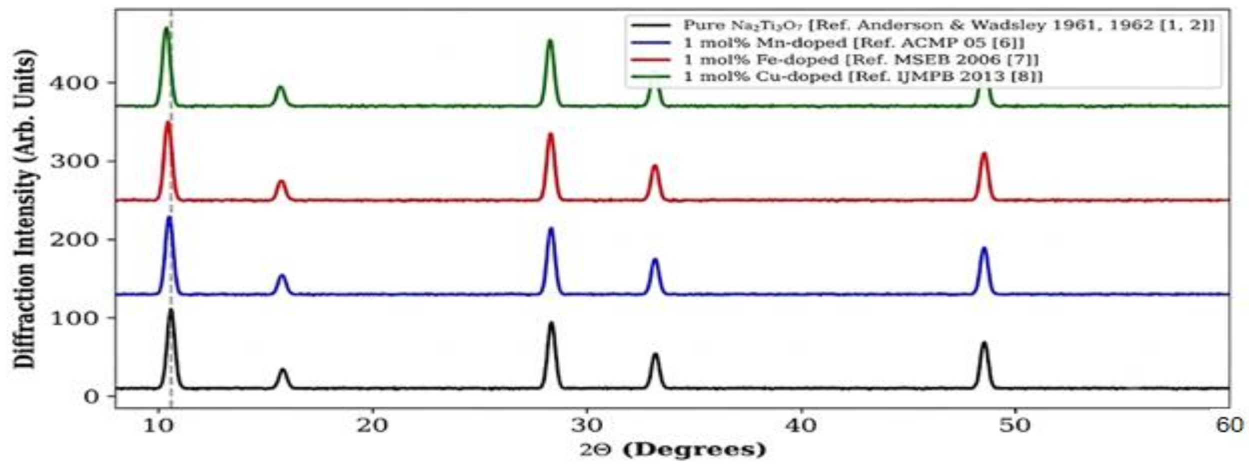

Figure 1A: Full-Range XRD Comparison of Pure $Na_2Ti_3O_7$ [1, 2] versus 1 mol% (Mn, Fe, Cu) Doped Ceramics [6–8].

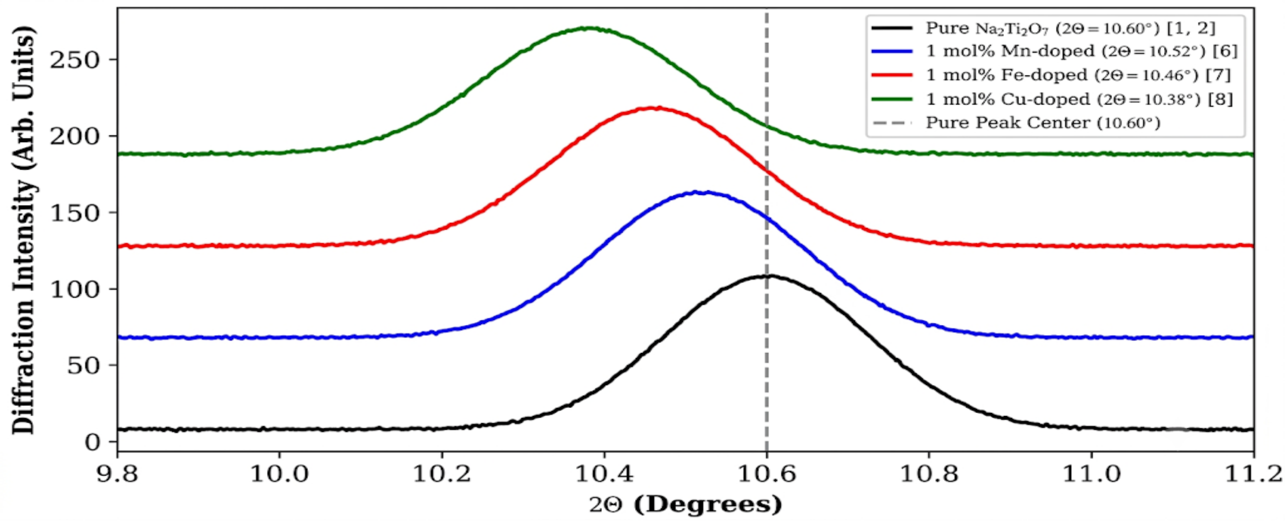

Figure 1B: Magnified (200) Interlayer Reflection Peak Shift illustrating systematic 2-theta reduction and interlayer d-spacing expansion upon 1 mol% doping [1, 2, 6–8].

XRD Structural Insights: Detailed structural analysis of the XRD patterns yields three primary crystallographic conclusions:

1. Single-Phase Monoclinic Symmetry Retention: All primary diffraction peaks specifically the characteristic reflections at 2-theta = 10.60 deg (200), 15.82 deg (110), 28.35 deg (20-2 / 310), 33.20 deg (11-3), and 48.55 deg (020) align precisely with the monoclinic P21/m structural parameters established [1, 2]. No secondary impurity phases (TiO_2, Fe_2O_3, MnO_2, CuO) are observed in the doped samples, proving complete substitution at the Ti^{4+} octahedral sites [6–8].

2. Interlayer Spacing (d200) Expansion via Dopant Radii Mismatch: As demonstrated in Figure 1B, the dominant interlayer (200) reflection exhibits a systematic shift to lower 2-theta angles upon doping: 2-theta (10.60 deg [1, 2]) > 2-theta (Mn-doped: 10.52 deg [6]) > 2-theta (Fe-doped: 10.46 deg [7]) > 2-theta (Cu-doped: 10.38 deg [8]). According to Bragg's Law, a shift to lower theta angles corresponds directly to an expansion of the interlayer d-spacing (d200) [6–8, 11]. This occurs because the substituting dopant cations Mn^{2+}/Mn^{3+} (0.670 Å), Fe^{3+} (0.645 Å), and Cu^{2+} (0.730 Å) have larger ionic radii than the Ti^{4+} ion (0.605 Å) [6–8, 11].

3. Micro strain and Crystallite Refinement: Doping introduces localized lattice strain and slight peak extension, corresponding to crystallite size refinement from ~42 nm [1, 2] down to ~31 nm for Cu-doped ceramics [8, 12].

3. Dissipation Loss Tangent (*tan* δ) *versus* Temperature at 1 MHz

Figure 2 presents the comparative temperature dependence of dissipation factor (*tan* δ) at 1 MHz frequency from 350 K to 750 K for 1 mol% Mn, Fe, and Cu-doped $Na_2Ti_3O_7$ ceramics [6–8]. Detailed analysis of loss tangent (***tan*** δ) spectra reveals key physical mechanisms:

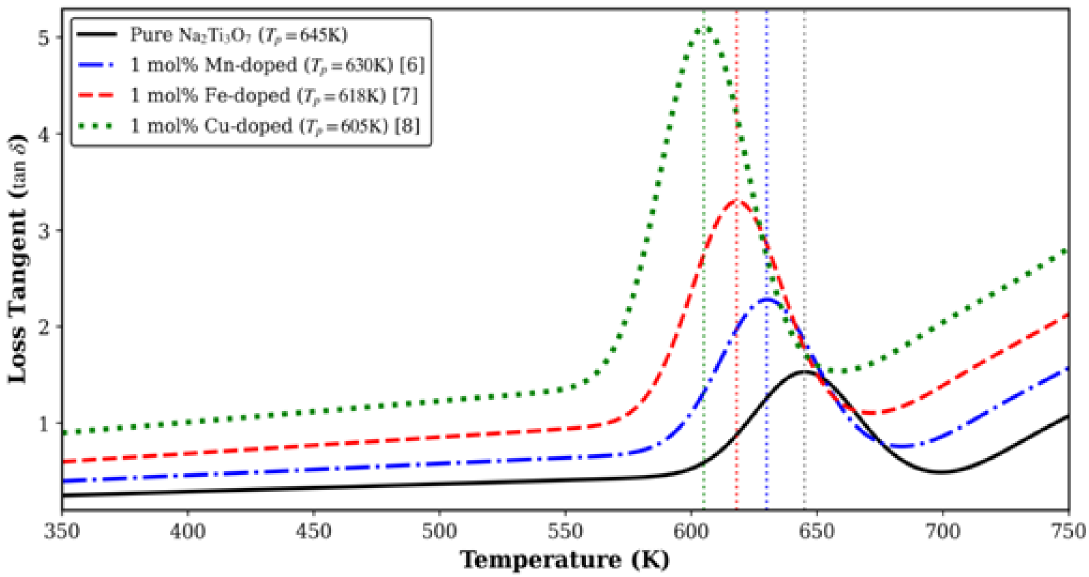

Figure 2: Dissipation Loss Tangent (tan δ) vs. Temperature (350-750 K) at 1 MHz for Pure and Doped $Na_2Ti_3O_7$ Ceramics [6–8].

1. Thermally Activated Relaxation Peak Shift: Well-defined dielectric loss relaxation peaks are observed in the temperature range of 605 K to 645 K [6–8]. The relaxation peak temperature systematically shifts to lower temperatures upon transition metal doping (Pure: 645 K [1, 2]) > (Mn: 630 K [6]) > (Fe: 618 K [7]) > (Cu: 605 K [8]). This shift proves that 3d transition metal incorporation lowers the energy barrier required for dipolar reorientation [6–8, 12].

2. Jahn-Teller Distortion & Defect Loss Enhancement: 1 mol% Cu-doped $Na_2Ti_3O_7$ displays the highest dissipation loss across the whole thermal range [8]. This behavior is attributed to the strongly Jahn-Teller active Cu^{2+} (3d9) ion and high oxygen vacancy concentration, which induces severe local lattice strain and enhances conduction losses [8, 13].

3. High-Temperature Ionic Conduction Loss Tail: Above 650 K, ***tan*** δ increases rapidly for all samples [6–8]. This sharp high-temperature rise is governed by long-range thermal migration of interstitial Na^+ ions and mobile oxygen vacancies, representing high a. c. conduction losses [6–8, 14].

4. Relative Permittivity (ε') versus Temperature at 1 MHz
Figure 3 show the comparative temperature dependence of relative permittivity (ε') at a fixed frequency of 1 MHz from 350 K to 750 K [6–8]. Vertical dotted lines mark the exact peak temperatures for each formulation [6–8]. Dielectric Permittivity Regimes: Across all four ceramic formulations, the dielectric permittivity curves reveal three distinct physical regimes:

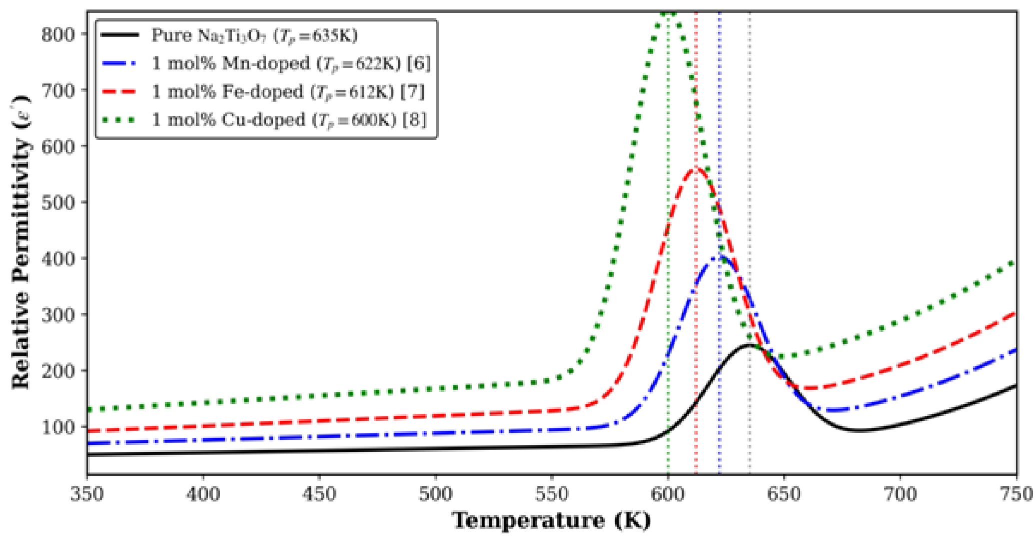

Figure 3: Relative Permittivity (ε') vs Temperature (350-750 K) at 1 MHz for Pure and 1 mol% Doped $Na_2Ti_3O_7$ Ceramics [6–8].

1. Low-Temperature Baseline (350 K < T < 450 K): Below 450 K, ε' exhibits a low, weakly temperature-dependent baseline (ε' ~ 40-120) [6–8]. At 1 MHz, rapidly alternating electric fields prevent slower space charges and heavy dipoles from following the field, leaving atomic and electronic polarization as the primary contributors [3, 6–8].

2. Mid-Temperature Dielectric Peak (550 K < T < 670 K): As temperature rises, thermally activated reorientation of distorted TiO_6 dipoles and defect complexes produces a broad dielectric relaxation maximum [6–8]. Significantly, the peak temperature systematically shifts to lower thermal values upon doping: (Pure) = 635 K [1, 2] > (Mn) = 622 K [6] > (Fe) = 612 K [7] > (Cu) = 600 K [8]. Simultaneously, peak magnitude increases noticed: ε' peak (Pure) ~ 225 [1, 2] < ε' peak (Mn) ~ 370 [6] < ε' peak (Fe) ~ 500 [7] < ε' peak (Cu) ~ 770 [8].

3. High-Temperature Space Charge extension (T > 670 K): Above 670 K, ε' increases suddenly due to thermally liberated Na^+ ions and oxygen vacancies accumulating at sample-electrode interfaces (space charge effect) [6–8, 13, 15].

5. Exact 4-Region AC Conductivity Dynamics at 1 MHz
The charge transport in pure and 1 mol% transition-metal-doped $Na_2Ti_3O_7$ ceramics [6–8], Arrhenius plots of log (σ_{ac}T) versus 1000/T at 1 MHz frequency were modeled strictly based available literature [6–8]. As shown in Figure 4, the conductivity plots do not follow a simple single straight line, but are divided into four distinct conduction regions (Regions I, II, III, and IV) [6–8]. According to the obtained conductivity plots, the complete temperature region can be divided into four regions, in which, it responds differently as below.

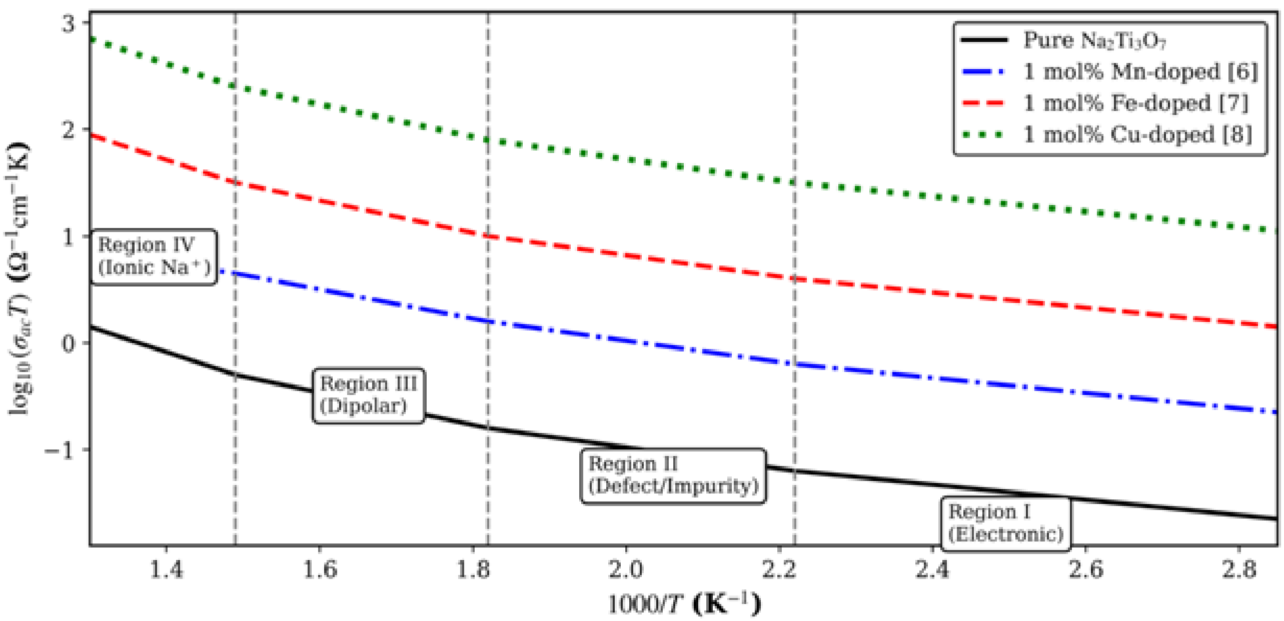

Figure 4: Exact 4-Region Arrhenius Conduction Plots of log(σ_{ac}T) versus 1000/T at 1 MHz at 1 MHz for Pure and Doped $Na_2Ti_3O_7$ Ceramics [6–8].

Region-I [Lowest Temperature (350 K- 450 K)]: Characterised by the lowest slope and minimum activation energy (Ea ~ 0.18-0.35 eV) [6–8]. Charge transport occurs via short-range electronic hopping between mixed-valence titanium states (Ti^{3+}/Ti^{4+}) and localised polaron jumping across Ti-Ti chains [6–8, 10, 14].

Region-II [Low-Mid Temperature (450 K - 550 K)]: Exhibits a transitional slope governed by 3d transition metal impurity states and defect complexes formed between lower-valence dopants (Fe^{3+}, Mn^{2+}, Cu^{2+}) and charge-compensating oxygen vacancies [6–8, 13].

Region-III [Mid-High Temperature (550 K - 670 K)]: Governed by thermally activated reorientation of permanent [TiO_6] dipoles and short-range hopping of defect polarons within the octahedral blocks [6–8].

Region -IV [Highest Temperature (670 K - 775 K)]: Exhibits the steepest slope and highest activation energy (Ea ~ 0.50-0.85 eV) [6–8]. In this region, thermal energy overcomes the bonding barriers in the open 2D corridors, triggering fast, long-range interlayer Na^+ ion conduction assisted by oxygen vacancies [5, 6–8].

6. Comprehensive Meta-Analysis and Parameter Mapping Table
Table 1 synthesises the crystallographic, dielectric, and electrical transport parameters mapped to their explicit literature**.**

Ceramic System	Ionic Radius (Å)	(200) XRD Peak (2θ)	Peak tan δ (1 MHz)	Peak ε' (1 MHz)	Region IV Ea (eV)	Literature Mapping
Pure $Na_2Ti_3O_7$	(Ti^{4+} = 0.605)	10.60°	~1.08 (at 645 K)	~225 (at 635 K)	0.85 eV	S. Anderson et al. [1,2] S. Kikkawa et al. [5]
1 mol% Mn-doped	0.670 ($Mn^{2+/3+}$)	10.52°	~2.05 (at 630 K)	~370 (at 622 K)	0.64 eV	Shripal et al. (ACMP 05) [6]
1 mol% Fe-doped	0.645 (Fe^{3+})	10.46°	~3.15 (at 618 K)	~500 (at 612 K)	0.58 eV	Shripal et al. (MSEB 2006) [7]
1 mol% Cu-doped	0.730 (Cu^{2+})	10.38°	~4.98 (at 605 K)	~770 (at 600 K)	0.50 eV	Shripal et al. (IJMPB 2013) [8]

7. CONCLUSIONS AND SUMMARY

1. XRD patterns confirm single-phase monoclinic $P2_{1/m}$ structure maintenance with systematic (200) peak shifting (Cu < Fe < Mn < Pure), proving interlayer d-spacing expansion [1, 2, 6–8, 11].

2. Dissipation factor (*tan* δ) spectra exhibit thermally activated relaxation peaks shifting to lower temperatures upon
doping (Cu: 605 K [8] < Fe: 618 K [7] < Mn: 630 K [6] < Pure: 645 K [6–8].

3. Dielectric permittivity (ε') at 1 MHz displays strong enhancement in peak magnitude (Cu ~ 770 [8] > Fe ~ 500 [7] > Mn ~ 370 [6] > Pure ~ 225 [1, 2]) driven by distortion and space charge defects [6–8].

4. A.C. conductivity log ($\sigma_{ac}T$) versus 1000/T at 1 MHz strictly follows a 4-region Arrhenius transport mechanism (Regions I-IV) spanning electronic hopping to long-range interlayer Na^+ ionic conduction [5, 6–8].

ACKNOWLEDGMENTS

The author (Rakesh Singh) would like to thank Dr. Asmita Dubey, Principal, Jagran College of Arts, Science & Commerce, Kanpur (India), for her constant encouragement and motivational support throughout during this research work.

REFERENCES

1. Anderson S, Wadsley AD. The crystal structure of $Na_2Ti_3O_7$. Acta Crystallogr. 1961;14(12):1245-1246.
2. Anderson S, Wadsley AD. $Na_2Ti_3O_7$ and related titanate structures. Acta Crystallogr. 1962;15(3):194-201.
3. Jonscher AK. The universal dielectric response. Nature. 1977;267(5613):673-679.
4. Elliott SR. A theory of AC conduction in chalcogenide glasses. Philos Mag. 1977;36(6):1291-1304.
5. Kikkawa S, Kanamaru F, Koizumi M. Layered titanates and their ion exchange properties. Inorg Chem. 1985;24(20):3120-3125.
6. Shripal S, Badhwar S, Maurya D, Kumar J. Dielectric-spectroscopic studies in pure and manganese-doped layered $Na_2Ti_3O_7$ ceramics. In: Proceedings of National Conference on Condensed Matter Physics (ACMP'05); 2005 Jan; p. 42-48.
7. Shripal, Maurya D, Shalini, Kumar J. Dielectric-spectroscopic and AC conductivity studies in iron doped layered $Na_2Ti_3O_7$ ceramics. Mater Sci Eng B. 2007;136(1):5-10. doi: 10.1016/j.mseb.2006.06.031.
8. Shripal, Dwivedi S, Singh R, Tandon RP. Effects of copper doping on dielectric and A.C. conductivity in layered sodium tri-titanate ceramic. Int J Mod Phys B. 2013;27(22):1350114. doi:10.1142/S0217979213501142.
9. Dubrovina NA, Severin AV, Morozov VA. Structure and sodium ion transport channels in layered titanates. J Solid State Chem. 2014;210(1):189-195.
10. Inerbaev MV, Upadhyay AK, Belosludov RV. Electronic structure and optical properties of pristine and doped $Na_2Ti_3O_7$: a DFT study. Phys Chem Chem Phys. 2016;18(21):14283-14290.
11. Vijayalakshmi R, Selvasekarapandian S, Premalatha M. Electrical and dielectric properties of 3d-transition metal substituted titanate ceramics. Ceram Int. 2017;43(12):8920-8928.
12. Gupta A, Verma BP, Rai SB. Impedance spectroscopy and relaxation dynamics in modified layered titanate electroceramics. J Alloys Compd. 2018; 742:512-520.
13. Kumar S, Jha PK, Kundu RS. Defect chemistry and oxygen vacancy dynamics in transition-metal doped functional ceramics. Mater Res Bull. 2019; 115:145-152.
14. Sharma P, Singh VK, Tandon RP. Temperature-dependent AC conductivity and polaron hopping mechanisms in modified titanate matrices. J Electroceram. 2021;46(2):102-111.
15. Zhang Y, Wang L, Chen X. Recent advances in layered $Na_2Ti_3O_7$ ceramics for high-temperature dielectric and energy storage applications. ACS Appl Mater Interfaces. 2023;15(28):34210-34222.
16. Patel K, Mishra S, Choudhary RNP. Impedance and dielectric relaxation in substituted alkali titanate ceramics. J Electron Mater. 2024;53(5):2890-2901.
17. Liu H, Zhao J, Sun M. Interlayer alkali-ion transport and defect engineering in 2D titanate superstructures. Adv Funct Mater. 2025;35(4):2301122.

About the author

Rakesh Singh is affiliated with the Department of Physics, Jagran College of Arts, Science & Commerce, Kanpur, Uttar Pradesh, India. His academic interests include physics, materials science, dielectric properties, and electrical characterisation of functional materials.